PHYSICAL FOUNDATIONS FOR DESIGN OF HIGH ENERGY BEAM ABSORBERS

A.Mikhailichenko, Cornell University, LEPP, Ithaca, NY 14853, U.S.A.

Abstract. We analyzed the physical basics for design of absorbers for high energy beams of electrons and photons. Typical examples are the collimators and dump systems. In particular, we considered a collimator for usage in Cornell ERL project, where it could be used for reduction of e^-, γ halo, minimization of exposure SRF module to SR from neighboring bending magnet and for absorption of direct beam hit in case of emergency. The collimator proposed uses Pyrolithic Graphite (PG) at front end and Tungsten insertion closer to the exit end. Beam dump system for absorption of 15 *MeV*, 1.5*MW* average power also uses a PG.

As examples we considered gamma collimator and gamma absorber (dump) for ILC positron conversion systems also.

1. OVERVIEW

Collimator is an inevitable component of any high-power electro-optical system. ILC and ERL are the most prominent examples of this kind.

ERL uses for recirculation of electrons: two DC SRF modules linked with CESR by electro-optical channel and by return loop at the other side [1]. Beam from injector module (~15 *MeV*) is directed into the first SRF module, which accelerates the electrons from 15 *MeV* to 2.5*GeV*. At the same time, the beam of 5 *GeV*, arriving from CESR site, transfers its energy into the same SRF module by deceleration to -2.5 *GeV*. After passage the ~180 deg return loop at the end of North SRF module, two beams (separated longitudinally by half wavelength) enter the second (south) SRF module. In this module, one beam continues its acceleration to 5 *GeV*, meanwhile the other beam continues its deceleration reaching ~10*MeV*. After that this low energy beam is separated from the high-energy one and directed into the beam dump, while the other beam, having energy ~5 *GeV* and low-emittance, goes to the experimental area and further to the CESR loop. After making a turn in CESR and channels, the beam enters the North SRF module and the process is repeated.

One place for the installation of a collimator could be identified at the entrance of the second (south) SRF accelerating section of ERL after the turning arc. One additional collimator of the same design-type (with complementary fast kicker in front of it) should be installed at the entrance of North linac. Another collimator (same design, but shorter) could be located nearby the Demerger. The same type of collimator(s) could be used for protection of low –aperture SR insertion devices. The arguments for this are straightforward.

To some extent, there is no self balanced mechanism of equalizing energies at the exit of North linac to 2.5*GeV* (and to 5*GeV* in experimental area) like it is in a cyclic machine with auto-phasing. The only parameter in hand is the controllable RF power from additional RF generators which makes the energy of one beam

higher, but the energy of other beam lower at the same time. The energy of one beam could be kept equal to the energy of another one by a sophisticated feedback system operating just this active RF power supply. This feedback system must analyze the energies of these bunches (and/or theirs currents and transform theses readings into RF feeding power.) Basically, one need to be prepared that the energies of two beams running in the return loop might be different and varying in time. This difference is defined by a dynamic range and functional stability of this feedback system in general[1].

Installation of collimator in front of South module, serves two purposes: *first* is to cut the halo of 2.5*GeV* beams (accelerated and decelerated) and, the *second*-to prevent the exposure of SC structure to SR from last bending magnet in the return loop. It was shown that this SR could deliver a problem, if not treated properly [2]. As far as the first function of the collimator–elimination of halo –it is straightforward. Some problems here might be associated with the fact that the typical distribution of the beam density in transverse direction is a Gaussian one only within few sigmas. The beam distribution then acquires wide wings extended up to the boundary of the vacuum chamber. Also, one need to keep in mind the possibility that this collimator must absorb at least one full train of bunches, beginning at the injector up to the entrance of the south SRF structure, which comes to n_b~5000 bunches (2500 from accelerating and 2500 from decelerating) each with a population up to $N \cong 4.8 \cdot 10^8$ (Q=77*pC*) at the E_0~2.5*GeV* carrying a total energy up to $E_{tot} \cong Q n_b E_0 \cong 1.9\ kJ$.

Collimator at the entrance of North SRF linac must be able to absorb ~two times this. As the beam size is extremely small, the density of energy deposition could destroy the material at once, if it is not protected properly. An undesirable situation could develop when the injector stops provision of the electron beam either due to SRF failure or if the photocathode stops generation of bunches. The latter might happen if either laser or HV system of the gun fails. In this scenario, the injected beam is absent, but the train from CESR arrives without interruption. The length of the train in this worst case scenario could reach the full circumference of system carrying ~10k bunches with 5*GeV* each having up to 77*pC*. All energy carried by these bunches $E_{tot} \cong 4\ kJ$ will be deposited, more likely, in the cryo-system, as in the absence of low energy beam all energy of decelerated (high-energy) beam goes for excitation of RF fields in SRF modules. Although the amount of Helium vaporized ~ 0.1 *kg* is not large[2], this will

[1] In principle one can consider some kind of auto-phasing, when the beam with different energy has different pathlength in CESR and channels, so while arriving to the entrance of North linac the bunches are shifted in phase so that they delivering different energy to RF fields. The same mechanism could be applied to the return loop. For these purposes the channels need to have some specific values of R_{56} matrix element. This pathlength difference could be controllable as an element of feedback also [3]. So depending on the arrival phase, additional RF power suppliers may deliver different power to the Cryomodule. *Indeed,* the return loop between North and South SRF modules must be isochronous, so at least R_{56} =0 here.

[2] Calculated with latent heat of vaporization of Helium ~21 *kJ/kg*.

immediately move the Helium from super-fluid state to an ordinary one in practically the entire line of Cryomodules. As such sudden energy deposition triggers the quench, the RF power of klystrons in addition to the stored energy in the RF fields may add to this as well. Namely, for the exclusion of this situation it is necessary to install a controllable beam dump at the entrance of North linac. This dump includes a collimator itself and a fast kicker, which directs the beam to the walls of the collimator in case of emergency. So, again, design of collimator must allow extension its functions so it becomes able to absorb full energy accumulated in many bunches. One must accept that ERL requires the presence of at least two collimators, able to withstand a direct hit of one full-circumference bunch train in its structure.

Similar problems appear in the design of collimators for ILC [4], although the beam energy carried by the train there at 250 *GeV* is much bigger, namely, $E_{tot} \cong eN_b n_b E_0 \cong 1.6 \cdot 10^{-19} \cdot 2 \cdot 10^{10} \cdot 2820 \cdot 250 \cdot 10^9 \cong 2.25 MJ$ in one train (~11 *MJ/sec*). Most results obtained here could be used for ILC as well, however. This is definitely true for gamma-collimator and gamma dump used in positron production system of ILC.

2. TO THE CHOICE OF DIMENSIONS FOR ABSORPTIONS OF ELECTRONS

The primary electron, positron or gamma beam with energy $E_0 >> mc^2$, when hitting the media, develops a cascade (shower), of what is a mixture of electrons, positrons and gammas accompanied by neutrons. Positrons created by gammas in electric field of nucleus of target material. Neutrons created by photonuclear reactions of different nature.

In simple dichotomy model, the cascade develops in the depth inside media from the point of penetration of initial beam; each step of multiplication in the shower associated with *radiation length* X_0.

$$X_0^{-1} \cong 4r_0^2 \alpha \frac{N_A}{A} Z(Z+1) \ln\left(\frac{183}{Z^{1/3}}\right) [cm^2/g], \quad (1)$$

A –is atomic weight of target substance, $N_A \cong 6.022 \cdot 10^{23}$ is the Avogadro number, Z is atomic number, $\alpha = e^2/\hbar c \cong 1/137$, r_0 is the classic electron radius.

The cascade propagates inside matter until energy of particles reaches the critical value,

$$E_c \cong \frac{610}{Z + 1.24}, MeV, \quad (2)$$

then the ionization losses become dominant. Transverse size of the cascade in its maximum is of the order of Molière radius

$$R_M \cong X_0 \frac{E_s}{E_c}, \quad (3)$$

where $E_s = \sqrt{4\pi/\alpha}\cdot mc^2 \cong 21.2\,MeV$–is a scale energy. Molière radius does not depend on energy of primary beam. Naturally, the Molière radius, expressed in cm, is bigger for lighter materials, as $R_M \approx 0.035\cdot Z\cdot X_0$ and $X_0 \propto A/Z^2$, so $R_M \propto A/Z$, where A is atomic weight. For W with its Z=74, $R_M^W \cong 2.57\,X_0$ (l_M^W =0.9cm), as the geometrical length corresponding to the radiation one is $l_{X_0} \cong 0.35cm$. For Ti, with its Z=22, $R_M^{Ti} \cong 0.7\,X_0$ (l_M^{Ti} =2.45cm), as $l_{X_0} \cong 3.55cm$, see Table 1 for more.

Table 1. Critical energy, radiation length, Molière radius for some elements

Elements →	C	W	Cu	Al	Ti	Fe
Z	6	74	29	13	22	26
A	12	183.8	63.5	27	47.9	55.8
E_c, MeV	84.2	8.1	20.2	42.8	26.2	22.4
X_0 g/cm^2	43.3	6.8	13	24.3	16.1	13.84
l_{X_0}, cm	19.2	0.35	1.45	9	3.58	1.75
R_M/X_0 (=E_s/E_c)	0.25	2.57	1.05	0.49	0.7	0.95
l_M, cm	4.8	0.9	1.5	4.4	2.5	1.65

The cascade (shower) reaches its maximum at the depth ($E_0 >> E_c$)

$$\frac{t_{\max}}{X_0} \cong \frac{1}{\ln 2}\ln\left(\frac{E_0}{E_c}\right) \tag{4}$$

with the number of particles (per each initial one) there around

$$N_{\max} \cong \frac{E_0}{E_c}. \tag{5}$$

Substituting in (4) E_0=5GeV for Carbon, E_c=82.4 MeV, one can obtain $l_{t_{\max}} \cong 115cm$, and the number of particles $N_{\max}$~60 (total of e^-, e^+, γ). Transverse size of the shower ~$l_M \cong 4.8cm$; these numbers give an idea of the dimensions required.

One can estimate geometrical volume occupied by cascade as

$$V_c \cong \frac{\pi}{3} l_{t_{max}} l_M^2 \cong \frac{\pi}{3\cdot ln\,2} l_{X_0}^3 \left(\frac{E_s}{E_c}\right)^2 ln\frac{E_0}{E_c} \propto l_{X_0}^3\cdot Z^2 \propto A^3/Z^4. \tag{6}$$

For example the ratio of these volumes for Tungsten and for Graphite becomes

$$\frac{V_c^C}{V_c^W} \cong \frac{l_{t_{\max}}^C}{l_{t_{\max}}^W}\left(\frac{l_M^C}{l_M^W}\right)^2 \cong \frac{115}{3.7}\times\left(\frac{4.8}{0.9}\right)^2 = 31\times 28 \approx 884, \tag{7}$$

i.e. the volume involved in a cascade inside C is about 900 times the volume inside W for the same initial energy of primary $5GeV$ electrons. Numerical value of volume for W is $V_C^W \cong \frac{\pi}{3} l_{t_{\max}} l_M^2 \cong \frac{\pi}{3} 3.2 \cdot 0.81 \cong 2.7 cm^3$, delivering density of energy deposition in W at least $P \cong E_{tot} / V_c^W / \rho \cong 4kJ / 51g \cong 78J / g$, what is only ~2 times lower, than a measured experimentally limiting density $P \le 180J / g$. As the real density of deposition at final points is bigger, than average one taken in above calculations, we can conclude, that Tungsten absorber is at the edge of survival.

As the circumference of ERL is about $C \cong 2420m$, period of revolution is $\tau_0 = C / c \cong 2420 / 3 \cdot 10^8 \cong 8\mu s$ and the total energy deposited in the target within this time. Full 5-GeV beam train corresponding average current I=0.1 A, carries energy $E_{tot} \cong IE_0 \tau_0 \cong$ 4 kJ (worst case scenario for collimator in front of North SRF linac). Now if all this energy deposited in a volume involved in a shower, the temperature rise for $E_{tot} \cong$ $4kJ$ deposition in Carbon will be $\Delta T \cong \frac{E_{tot}}{mC_p} \cong \frac{E_{tot}}{\rho \frac{\pi}{3} l_{t_{\max}} l_M^2 C_p} \cong 1.2^o K$ only, where $C_p \cong 0.71$ $J/g/^o K$ is a heat capacity of Carbon, and $\rho \cong 2.25 g / cm^3$ was taken as its volume density[3]. So the Graphite absorber will survive a direct hit of train in contrast with the one made from Tungsten (or Iron). Even so the high local power density may deliver a problem at the incident point, as the shower is not developed yet there, see below. Also, one of the operational modes has the beam charge suggested ~$10nC$ at lowered repetition rate, so each single bunch carries $N_b \cong 10nC / 1.6 \cdot 10^{-19} C \cong 6.25 \cdot 10^{10}$ electrons and energy $E_{tot} \cong 10nC \cdot 5GeV = 50J$.

The temperature profile repeats the profile of shower and the thermal pressure p_T can be expressed as the following [19]

$$p_T = \Gamma(V) \frac{c_V T}{V} = \Gamma(V) \frac{\varepsilon_T}{V}, \qquad (8)$$

where coefficient $\Gamma(V) = V / c_V (\partial P / \partial T_V)$ ~1.5-2 which characterizes the ratio of the thermal pressure p_T to the specific thermal energy ε_T / V called Grüneisen coefficient. By introduction of thermal expansion coefficient α_T, Grüneisen coefficient can be expressed as

$$\Gamma(V) = V \alpha_T K_T / c_v = V \alpha_T K_S / c_P, \qquad (9)$$

where K_S is the adiabatic bulk modulus. Let us consider an interaction of this bunch when it hits a thin wall, what might be a wall of vacuum chamber. If the beam size defined by local values of envelop function β , then its size comes to

[3] For Tungsten this temperature rise is, formally, $\Delta T \cong 600^o K$.

$\sigma_{\perp}^2 \cong (\gamma\varepsilon)\cdot\beta/\gamma$. If the thickness of the wall is $l_w << l_{t\max}$ then the volume involved is $V \cong \pi l_w(\gamma\varepsilon)\cdot\beta/\gamma$, where $\gamma\varepsilon$ stands for invariant emittance. If the volume density of material of the chamber is $\rho[g/cm^3]$ then the energy deposited in a wall by all particles could be evaluated $\varepsilon_T \cong N_b \cdot 2[MeV/(g/cm^2)]\cdot l_w \cdot \rho$. So the pressure existing at the very first moments comes to [6]

$$p_T = \Gamma(V)\frac{\varepsilon_T}{V} \cong \Gamma(V)\frac{N_b \cdot 2\cdot\rho\cdot\gamma}{\pi\cdot\gamma\varepsilon\cdot\beta}, \qquad (10)$$

where *z* coordinate runs from the entrance of target. One can see, that thickness of the wall l_w disappeared from the final formula: energy deposition is proportional to l_w, the same is the volume. For $\gamma\varepsilon \cong 0.1mm\cdot mrad = 10^{-5}cm\cdot rad$, $\beta \cong 10m = 1000\ cm$, $\rho \cong 19.1g/cm^3$ (W), $\Gamma \cong 2.4$, the pressure comes to

$$p_T = \Gamma(V)\frac{\varepsilon_T}{V} \cong 2.4\frac{6.25\cdot10^{10}\cdot2\cdot10^6\cdot19.1\cdot10000}{\pi\cdot10^{-5}\cdot1000} = 2.9\cdot10^{23}\ [eV/cm^3].$$

The last number could be expressed

$$p_T \equiv 2.9\cdot10^{23}\frac{eV}{cm^3} \equiv 4.64\cdot10^4\frac{J}{cm^3} \equiv 4.64\cdot10^{11}\frac{erg}{cm^3} \cong 4.64\cdot10^{11}\frac{dyne}{cm^2} \equiv 464kBar,$$

meanwhile the elasticity of W is limited by 1.08 *kBar*. This example indicates how serious the problem associated with small transverse cross section might be even for a single bunch.

More complicated cascade theory includes details of the process. For normal entrance in media, the distribution of density of particles in transverse dimensions characterized by NKG (after Nishimura-Kamata-Greisen) function [5]

$$F(r) = K(s)\frac{r^{s-2}}{R_M^s}\left(\frac{r}{R_M}+1\right)^{s-4.5}, \quad K(s) = 0.443s^2(1.9-s),\ s<1.6 \qquad (11)$$

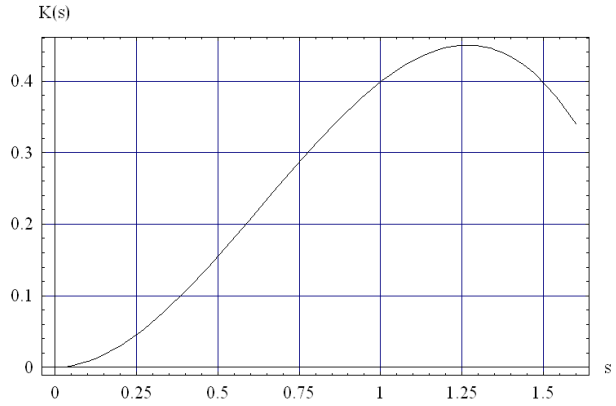

Figure 1: Longitudinal profile of shower, *K*(*s*).

where r stands for the radial distance from the axis of shower, s is its age (defined by (19), see below).
So the number of particles $N(r,t(s))$ in limits of radius r could be obtained as

$$N(r,t(s)) = N(t(s)) \cdot \int_0^r F(r')2\pi r' dr' \ , \tag{12}$$

where $N(t(s))$ total number of particles in a shower at the depth t defined by s.

Initial transverse beam distribution supposed a delta-function so far. For finite transverse dimensions for the beam having distribution at the entrance as $f_0(r_0)dr_0^2$ the distribution function at the depth $t=t(s)$ could be found as

$$f(\vec{r})d^2\vec{r} = \int f_0(r_0)F(r')d^2\vec{r}_0 d^2\vec{r}', \quad \text{while } \vec{r} = \vec{r}_0 + \vec{r}' \tag{13}$$

For Gaussian initial distribution

$$f_0(r_0) = \frac{1}{\pi < r_0^2 >} \exp\left(-\frac{r_0^2}{< r_0^2 >} \right) \tag{14}$$

function $f(r)$ has a form

$$f(r) = \frac{1}{\pi < r_0^2 >} \int_0^\infty F(r') \exp\left(-\frac{r^2 + r'^2}{< r_0^2 >} \right) \cdot I_0\left(\frac{2rr'}{< r_0^2 >} \right) \cdot 2\pi r' dr' \ . \tag{15}$$

At the axis of shower ($r=0$), this expression could be simplified to

$$f(0) = \frac{1}{\pi < r_0^2 >} \int_0^\infty F(r') \exp\left(-\frac{r'^2}{< r_0^2 >} \right) 2\pi r' dr' . \tag{16}$$

The last expression could be further simplified for $< r_0^2 > << R_M^2$ by direct integration [6]

$$f(0) = \frac{1}{\pi < r_0^2 >} \pi K(s) \Gamma\left(\frac{s}{2} \right) \left(\frac{< r_0^2 >}{R_M^2} \right)^{s/2} \tag{17}$$

Ratio of axial density at the depth t to the density at the entrance both measured at the axis goes to be

$$\frac{d^2N(t,r)}{dr^2} \Big/ \left. \frac{d^2N(0,r)}{dr^2} \right|_{r=0} = \pi < r_0^2 > f(0)N(t) \cong \pi K(s) \frac{< r_0^2 >^{s/2}}{R_M^s} \Gamma(\tfrac{s}{2}) N(t(s)) \tag{18}$$

By introduction of variables

$$\eta = \ln \frac{E_0}{E}, \quad \eta_0 = \ln \frac{E_0}{E_c}, \quad x = \ln \frac{r}{R_M}, \tag{19}$$

where E stands for the current energy of particle, the age of shower could be expressed as [5]

$$s \cong \frac{3t}{t+2\eta} = \frac{3t}{t+2\eta_0+2x}, \tag{20}$$

where the depth t is measured in fractions of X_0 now. Physical meaning of variable η is clear, as the energy dependence is $E = E_0 \exp(-\eta)$.

The number of particles at the depth t and energies grater than E, while initial one was E_0 (all measured in units of critical energy now) goes to be [5]

$$N(E_0, E, t) \cong \frac{0.135}{\eta^{1/2}} \exp[t(1-\tfrac{3}{2}\ln s)], \tag{21}$$

so the total number of particles comes to

$$N(E_0, E=0, t) \cong \frac{0.31}{\sqrt{\eta_0}} \exp[t(1-\tfrac{3}{2}\ln s)]. \tag{22}$$

In fractional to X_0 units, this expression practically does not depend on material nature. At the shower maximum s=1, according to(16), (17), $t = t_m \cong \eta$, in good agreement with results of simple dichotomy theory (4).

The number of particles having energy >E could be expressed as $N(E_0, E, t) \propto E^{-s}$. At shower maximum, $s \cong 1$ [5]

$$N_{\max}(E_0, E) \cong 0.31 \frac{E_0}{E_c} \frac{\phi(2.3E/E_c)}{\sqrt{\eta_0}}, \tag{23}$$

Where function $\phi(y) \cong \frac{1}{y}(1-\frac{2}{y}+..)$, $y > 1$. This formula shows, that the number of particles with some threshold energy is a few times less, that the total number of particles predicted by formula (5).

Oblique hit the wall under small angle ϑ considered in [6]. Below we represent some results from there useful in collimator design. In this case the effective length of entrance spot $L \cong r_0 / \vartheta$ is much more than the distance corresponding development of shower and the distribution of particles in the wall becomes equilibrium with

$$N(r, E) = \int N(r, E, t) dt. \tag{24}$$

Total number of particles in cross section of this shower defined by the balance of number of primary particles entering the wall of collimator per unit length

$$\frac{dN_0}{dx} \cong n_0 \sqrt{2} \cdot r_0 \vartheta, \tag{25}$$

where n_0 stands for the particle density in cross section of incoming beam, $\sqrt{2}\, r_0$ stands for effective width of the beam and by the energy losses by ionization process at the radiation length so

$$N_{eq} \cong n_0 \sqrt{2}\, r_0 \vartheta X_0 \frac{E_0}{I} \tag{26}$$

where I is the rate of ionization losses. The last one for E_0=2.5 *GeV*, r_0=0.6mm and bunch population $N_b \cong 6.25\cdot 10^{10}$ (10nC) in Copper

$$N_{eq} \cong 7.8\cdot \vartheta \cdot 10^{13}. \qquad (27)$$

The width of the shower reaches $\sqrt{< r^2 >} \cong R_M$, however, so the energy density is not high, but the peak of particle density and density of energy deposition manifests itself at the distance $\sim \vartheta t_m$ counted from the surface of material.

Distribution of particles in a wall as function of depth y, counted from the surface, could be expressed as

$$f(x,y) = n_0 \int f_0(x_0, y_0)\cdot F(\sqrt{(x-x_0)^2 + (y-y_0)^2}\, dx_0 dy_0 \qquad (28)$$

where $f_0(x,y)$ is a transverse distribution of particles at the entrance, n_0 defined at x_0 =0, y_0 =0 , function $F(r)$ represented at (11). Coordinate y_0 related to the age of shower by $y_0 = \vartheta \cdot t(s)$, where dependence $t(s)$ calculated from the entrance, defined by (20). If the beam size in y direction is bigger, than $y_0 = \vartheta \cdot t_m$, then function f could be carried out of integral and account it as $n_0 \to n_0(y)$. If intial distribution is a Gaussian one, with dispersions $< x_0^2 >$ and $< y_0^2 >$, so $\sqrt{< y_0^2 >} >> \vartheta t_m$, then

$$f(x,y) = n_0(0,y)\int \exp\left(-\frac{x_0^2}{<x_0^2>}\right)\cdot F(\sqrt{(x-x_0)^2 + (y-y_0)^2}\, dx_0 dy_0 . \qquad (29)$$

The last expression could be integrated for x=0 (at the center of the beam axis), so finally

$$f(0,y) = n_0(0,y)\int_0^{\infty} \left(-\frac{<x_0^2>}{R_M^2}\right)^{\frac{s-1}{2}} \cdot \Gamma(\tfrac{1}{2}) K(s)\left\{\xi^{\frac{s-1}{2}} \cdot \frac{\Gamma(\frac{s+1}{2})}{\Gamma(1-\frac{s}{2})} + \frac{\Gamma(\frac{s+1}{2})}{\Gamma(\frac{1}{2})}\right\}\frac{dy_0}{R_M}, \qquad (30)$$

where it was introduced $\xi = \frac{(y-y_0)^2}{2 < x_0^2 >}$.

For $\vartheta = 10^{-5}$, $\sqrt{2 < x_0^2 >} = 6.3\cdot 10^{-2}\, cm$ in Copper, the density of shower at the surface (y=0) is ~three times the bunch density. Maximum of density located at the depth $\sim 7\cdot 10^{-5}$ *cm* and is ~1.5 times bigger, than at the surface. In the number of particles in a bunch is $N \cong 6.25\cdot 10^{10}$, the temperature rise will be ~18.7°C per pulse. For the train of 2500 bunches, taken as estimation of length of the train, the temperature rise comes to 47000 °C. Formally Copper will be melted after ~1083/18.7~58 bunch in the train sequence. Entrance of tails of radial distribution off setting by $\sqrt{2 < x_0^2 >}$ from center will raise the temperature ~2.5 °C per bunch, so the train of 2500 will heat the material up to 6250 °C.

One additional important moment here associated with the generation of plasma around the incident point or line in the case of an oblique hit. Atoms of vaporized metal become immediately ionized along the line nearby the wall hit, so the ions could compensate the space charge inside impact bunch. This plasma lens developed quickly as typical speed of ions is around v_p ~1mm/μsec and for micrometer-size beam compensation established during a fraction of a nanosecond while the beam duty in ERL could reach 8μs as we mentioned above. This might be especially dangerous in case of oblique hit as the acting distance for this ion lens is big and the high energy beam might be focused to extremely small transverse cross section.

That is why we suggesting usage of low *Z* material in front end of collimator. Pyrolithic Graphite emerges as a best candidate for these purposes.

3. TO THE CHOICE OF DIMENSIONS FOR COLLIMATION OF PHOTONS IN ERL

As it was mentioned in Overview, the second function of collimator is in protection of SC structure against exposure to SR from the last bending magnet of return loop. Schematic view of hardware around collimator is shown in Fig. 2 below.

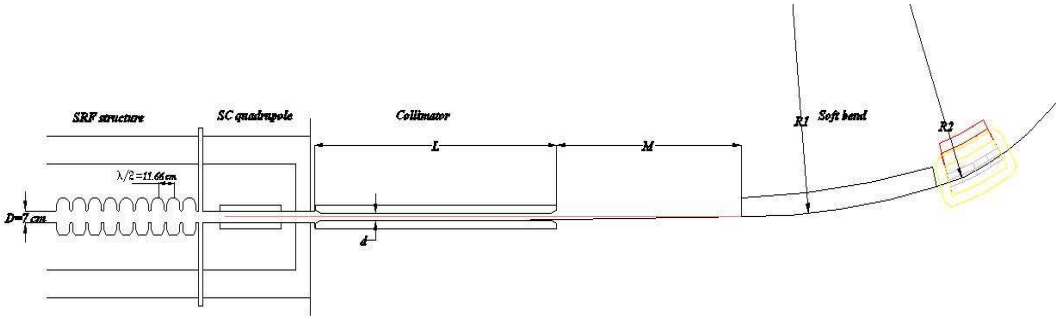

Figure 2: Top view to the collimator region. Beam is coming from the right.

We reserved some space between collimator and the edge of last bending magnet for installation of focusing elements; this space marked as *M* in Fig.2. Scaled view represented in Fig. 3.

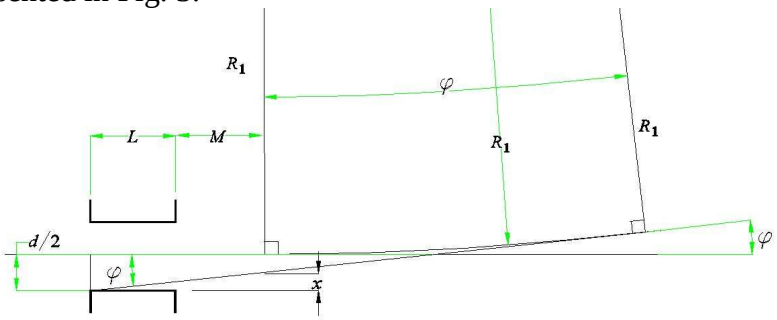

Figure 3: To the definition of limiting irradiation angle φ.

The last magnet of the bending loop (at the right) is split in two sections having bending radiuses R_1 and R_2 respectively; so $R_1>>R_2$. If diameter of collimator is d, its length is L, distance between collimator and the last magnet edge M, then the value of azimuthtal angle φ which sees inside SRF cryomodule could be found from the system of exact equations, Fig.3

$$\left.\begin{aligned}(R_1+\frac{d}{2}-x)\cos\varphi &= R_1\\ \tan\varphi &= \frac{x}{L+M}\end{aligned}\right\}. \tag{31}$$

Despite the system looks rather simple, its exact solution, which could be found, say, with Mathematica©, looks extremely complicated[4]. That is why we will use approximation

$$\varphi \cong \frac{d}{4(L+M)}. \tag{31a}$$

The number of photons radiated by each particle *within* this angle goes to be

$$N_\gamma \cong \alpha\gamma\varphi \cong \frac{\alpha\gamma d}{4(L+M)}, \tag{32}$$

whrere $\alpha = e^2/\hbar c \cong 1/137$ is a fine structure constant.
As characteristic energy of each photon is

$$\hbar\omega_c = \tfrac{3}{2}\frac{\hbar c}{R_1}\gamma^3 = \tfrac{3}{2}mc^2\frac{\lambda\!\!\!^{-}_C}{R_1}\gamma^3, \tag{33}$$

where $\lambda\!\!\!^{-}_C = \frac{e^2}{mc^2}\frac{\hbar c}{e^2} = 3.86\cdot10^{-13}m$ is e^- Compton wavelength/2π. Total energy deposited by each particle inside SRF comes to

$$E_{tot} \cong \tfrac{3}{8}mc^2\frac{\alpha\lambda\!\!\!^{-}_C d}{R_1(L+M)}\gamma^4 \tag{34}$$

If we accept for estimation R_1=100 m, L=1m, d=1cm, $\gamma \cong 5000\,(2.5GeV)$, then $E_{tot} \cong \tfrac{3}{8}mc^2\frac{3.86\cdot10^{-13}0.01}{137\cdot100\cdot(1+1)}625\cdot10^{12} \cong 1.3\cdot10^{-4}\cdot mc^2 \cong 16.6\ eV$. As the current expected to be I=0.1A, then the power deposition comes to P~1.65W. Meanwhile energy of quanta is, according to (33), $\hbar\omega_c \cong 7.2\cdot10^{-4}\cdot mc^2$ i.e. radiation is in statistical regime, as the number of quantas radiated is less, than one, $N_\gamma \cong \frac{\alpha\gamma d}{4(L+M)} \cong \frac{5000\cdot0.01}{137\cdot8} \cong 0.046$ per electron.

[4] It is interesting, that it is not possible to expand cos or tan here.

About the same power will be deposited is a collimator itself. As the vertical size of photon flux will be $\Delta y \cong (L+M)/\gamma \cong 4\cdot 10^{-4} m \equiv 0.4mm$, the power comes to

$$\frac{P}{Area} \cong \frac{1.65W}{0.4mm\cdot 1000mm} \cong 0.004W/mm^2 (\equiv 4kW/m^2),$$

which is not big for collimator. Radiation first touches the SRF at the distance

$$\tilde{L} \cong L\frac{D}{d}. \tag{35}$$

For example, if D=7 *cm*, then $\tilde{L} \cong 7m$ i.e. somewhere inside second module. As the power ~1.66*W* distributed evenly at the distance starting from 7 meters behind collimator up to the infinity, the density of power deposition in horizontal direction drops linearly with distance *r*. In addition to this, as vertical size of the photon flux increased ~r/γ, then the power density drops ~$1/r^2$ and at first touch is ~49 times smaller, than the power density at the inner surface of collimator, i.e. ~$8\cdot 10^{-5}$ *W*/*mm*^{2}=80 *W*/*m*^{2}, which is acceptable according to [1].

Shadow of iris defines the fraction of energy deposited in each iris around first touch as

$$\delta \cong \frac{\lambda}{2}\frac{d}{4(L+M)}, \tag{36}$$

where $\lambda/2$ $(\cong 11.6cm)$ stands for the period of structure. So the illuminated area on iris collects radiation within angle

$$\tilde{\varphi} \cong \frac{\delta}{\tilde{L}} = \frac{\lambda d^2}{4(L+M)LD} \tag{37}$$

So the total number of photons (per electron) falling on the iris goes to be

$$N_{\gamma iris} \cong \tilde{\varphi}\alpha\gamma \cong \frac{\delta\alpha\gamma}{\tilde{L}} = \frac{\alpha\lambda d^2\gamma}{4(L+M)LD}, \tag{38}$$

which carry the energy

$$E_{\gamma iris} \cong \tfrac{3}{2}mc^2\frac{\hat{\lambda}_C}{R_1}\frac{\lambda d^2\gamma^4}{4(L+M)LD}. \tag{39}$$

Total power illuminating the iris comes to

$$P_{\gamma iris} \cong \tfrac{3}{2}mc^2\frac{\alpha\hat{\lambda}_C}{R_1}\frac{\lambda d^2\gamma^4 I}{4(L+M)LD}. \tag{40}$$

And, finally, the power density comes to the value

$$\frac{P_{\gamma iris}}{Area} \cong \tfrac{3}{2}mc^2 I\frac{\alpha\hat{\lambda}_C}{R_1}\frac{\tilde{\varphi}\gamma^4}{\tilde{\varphi}\tilde{L}}\cdot\frac{\gamma}{\tilde{L}} = \tfrac{3}{2}mc^2 I\frac{\alpha\hat{\lambda}_C\gamma^5}{R_1}\left(\frac{d}{LD}\right)^2 \tag{41}$$

If bending radius of last magnet is R_1, then φ defines the minimal magnetic length of soft bend magnet

$$l_s \cong R_1 \cdot \varphi \cong R_1 \frac{d}{4(L+M)} \cong 100 \frac{0.01}{8} = 0.125m\,. \qquad (42)$$

From an engineering point of view, the soft part of the bending magnet, having radius R_1, could be made longer than this minimal value defined by (42) with minimal efforts; so from this point, the length of three-four times bigger is more preferable, coming to ~50cm.

Photon collimation of gammas in ILC has some peculiarities [4]. First of all, the photons have energy defined by undulator spectra, with the first harmonic around 10-15 MeV much below critical energy for C. Second –the beam after collimator could be not so clean from scattered particles, as the target is a room-temperature device. Neutron generation in this tandem reduced in first place by high threshold neutron Photoproduction cross section in Carbon.

Attenuation of gammas in ILC gamma-collimator is going through Compton scattering mostly at high energy (≥ 0.1MeV) coming to $I^{\gamma} = I_0^{\gamma} \cdot \exp(-t/\lambda_{att})$ with absorption length $\lambda_{att} \cong 10 g/cm^2$ [19]. For Graphite this comes to $l_{att} \cong 5cm$. So the Graphite section comes to $\cong 10 l_{att}$ ~50cm followed by ~7cm of Tungsten insertion. At the moment of arrival to the Tungsten section the gamma inensity reduced by a factor $\sim 2 \cdot 10^4$.

4. NEUTRON FLUX

Neutrons are generated as a result of so-called *photonuclear reactions* mostly. Mean lifetime of a neutron is 885.7 seconds (14.8min) and it decays to a proton, electron and anti-neutrino (100% branching). Neutrons classified by theirs energy E as the following:

1) Slow neutrons – E<1 keV
2) Neutrons of transition energy–1keV<E<0.2MeV
3) Fast neutrons –0.2MeV<E<20MeV
4) Ultra-fast neutrons –E>20MeV.

Reaction of photo-production has a threshold, which depends on media. For Tungsten, the gammas with energy E< 6.19 MeV can not generate neutrons [8]; for reaction of (γ, 2n) the threshold is 13.6 MeV (in W). For some materials thresholds represented in Table 2.

Table 2: Threshold energy for (γ, n) reaction.

Elements →	C	W	Cu	Al	Fe	Pb	U
$E_{\gamma h}(\gamma,n)$, MeV	18.72[5]	6.19	9.91	13.03	11.21	6.73	6.04

[5] Natural Graphite contains 1.1% of C^{18} which has a threshold of 4.9 MeV for (γ,n) reaction [17].

One can see from this table that the beam dump suggested for ERL containing Graphite as absorber (paragraph 7 below), *will not generate neutrons at all*, if the dump energy of the beam remains below 18 MeV.

In Lead, experimentally measured yield of neutrons in region of 1.25 *GeV* comes to be ~0.6 neutron/electron in a target which is~3 *cm* thick [9]. According to [9] the yield after reaching this thickness does not depend on the thickness anymore (saturated yield). For 230-*MeV* electrons the yield measured is proportionally lower.

In [8] represented photonuclear reaction yields for gamma-production as function of energy and material. About 99.98% of gammas participate in neutron creation, so reduction of gamma-flux is a priority task for our purposes. It is shown, that the yield comes to saturation above energy of incoming gammas above ~40 *MeV*. The ratio of rates in neutron production is strong function of *Z* and comes to ~20 for Tungsten vs Graphite. Neutron yield in Iron is ~5 times bigger, than for Graphite. Energy spectrum of neutrons drops rapidly beyond 13 *MeV* and has drop ~100 times beyond first threshold energy (~6.19*MeV* for W). At maximum, which happens at low energy (<0.1MeV) yield reaches 10^{-2} for each irradiating electron having energy100*MeV*.

In principle one can take the formula (22) for the number of the particles and multiply this number by the cross section for photo-production for obtaining the number of neutrons. *We will apply a different approach, developed for these purposes.* This approach includes the concept of differential track length.

The number of neutrons produced by initial electron could be expressed as [12]

$$Y(E_0)=\frac{N_A\rho}{A}\int_{E_{\gamma th}}^{E_0}\sigma_n(E_\gamma)\frac{dL^\gamma(E_0,E_\gamma)}{dE_\gamma}dE_\gamma\equiv\frac{N_A\rho}{A}<\sigma_n(E_\gamma)L(E_0,E_\gamma)>_E, \quad (43)$$

where $E_\gamma=\hbar\omega$ is the photon energy, dL^γ/dE_γ is the photon differential track length, $\sigma_n(E_\gamma)=\sigma(\gamma,n)+\sigma(\gamma,np)+2\sigma(\gamma,2n)+...$ is a sum of partial cross sections for neutron production [15]. [16]. Definition of dL^γ/dE_γ is clear from right side of (39) and is nothing else but the value of track length averaged over energy. The photon differential track length is

$$\frac{dL^\gamma(E_0,E_\gamma)}{dE_\gamma}=\frac{F^\gamma}{E_\gamma}\frac{X_\gamma}{X_0}\int_{E_\gamma}^{E_0}\frac{dL^e(E_0,E_\gamma)}{dE}F^e dE \quad (44)$$

where $X_\gamma=A/(N_A\rho\sigma_\gamma)$ stands for the photon relaxation length, so $X_0/X_\gamma\cong\frac{7}{9}$, F^e and F^γ are correction factors, ~0.7-0.9 depending on the material and energy, dL^e/dE is differential track length for electrons. Electron differential track length defined by [13]

$$\frac{dL^e(E_0,E)}{dE} = \frac{E_0}{0.437}\frac{X_0}{E_C^2}\left[\frac{1}{\kappa} - (1+\kappa)e^{\kappa}\cdot\int_{\kappa}^{\kappa_0}\frac{e^{-s}}{s^2}ds\right] \qquad (45)$$

where $\kappa = E/0.437E_C$ and $\kappa_0 = E_0/0.437E_C$. Equations (43)-(45) allow calculation of yield for different initial energy of electron. Formula (43) could be approximated as the following

$$Y(E_0) = 0.572\frac{N_A\rho X_0 E_0}{A}\int_{E_{\gamma h}}^{E_0}\frac{\sigma_n(E_\gamma)}{E_\gamma^2}dE_\gamma, \qquad (46)$$

Showing that the input of high energy gammas in yield suppressed as $\sim 1/E_\gamma^2$.

Results of numerical integration of (43)-(46) represented in Table 3.

Table 3 [11] Neutron yields in units of 10^{12} neutrons/sec/kW for the target with thickness $\geq 3X_0$

Elements →	C	W	Cu	Al	Fe	Pb
E_0=34 MeV	0.097	1.98	0.074	0.22	0.51	1.6
E_0=100 MeV	0.31	2.28	1.03	0.50	0.72	1.85
E_0=500 MeV	0.38	2.42	1.08	0.56	0.76	1.98
E_0=1000 MeV	0.38	2.42	1.08	0.56	0.76	1.98
E_0=6.3GeV [14]	-	-	2.2	1.1	-	2.6

One can see, that the yield saturated after E_0>100 MeV. So now we can express the neutron yield as [11]

$$Y(n/\text{sec}/kW) \cong 9.3\cdot 10^{10}\cdot Z^{0.73\pm 0.05} \quad . \qquad (47)$$

Spectrum of neutrons located mostly below the threshold for (γ, 2n), as the number of high-energy photons is exponentially lower at higher energy, and as a result of decrease of cross section beyond resonance pick. Experimentally measured spectrum represented in Fig.4 for 100-MeV incident electrons [8].

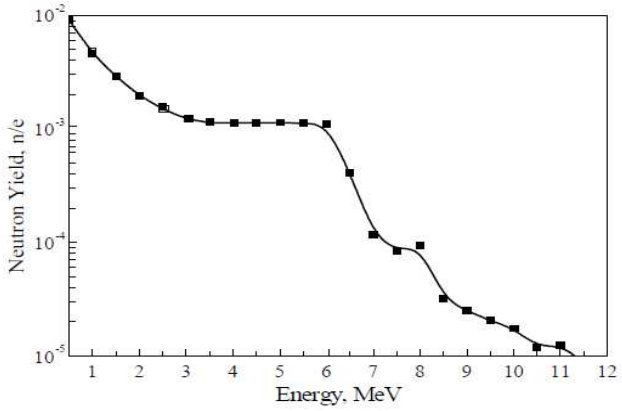

Figure 4: Energy spectrum of neutrons created by 100-MeV electrons in W [8].

One can see, that neutron yield drops ~1000 times behind 11*MeV* for 100-*MeV* primary electrons.

It is easy to understand the suppression of high-energy neutrons in spectrum. To acquire high energy, each of three quarks (*u*,*d*,*d*) needs to be accelerated to about the same energy. As electric field of the photon acts differently to the up and down quarks (having charge 2/3*e*, -1/3*e*), more probable becomes accelerating just one quark, which needs to be dressed by anti-quark, so some channel might be the one going through light mesons ($\pi^{\pm,0}$), suppressed by necessity to create this anti-quark. At low photon energy, the energy acquired by a single quark, could be re-distributed among other two by strong force, which is ~$1/\alpha$ times bigger, than the electromagnetic one.

So even taking into account that energy of ultra-fast neutrons is proportionally higher, total input into energy deposition of these neutrons remains below 10%. Some rise in low part of spectra is explained by populating this part of spectra by neutrons scattered by media and lost their energy. For higher energy of incident electrons the shape of graph remains the same, so the fraction of ultra-fast neutrons remains the same if normalized to the full neutron yield, so one can expect, that formula (47) for the yield includes all this.

For 1 *nA* loss of 5*GeV* beam (so power loss is 5*W*=0.005 *kW*), formula (47) gives $Y \cong 9.3\cdot 10^{10}\cdot 3.7\cdot 5\cdot 10^{-3} \cong 1.7\cdot 10^{9}$ neutrons/sec for Carbon. *For Tungsten the yield is 6.26 times bigger.* Knowing the yield of neutrons one can calculate the dose, associated with neutron flux at distance *R* from the source [11]

$$\dot{D}(rem/hour) \cong 93\cdot Z^{0.73}\,\frac{P[kW]}{R[m]^2}\ . \qquad (48)$$

So the dose for 1 *nA* local losses in Carbon comes to be $\dot{D} \cong 0.43$ rem/hour at the distance *R*=2 *m* unshielded. So, adequate neutron protection is required for the collimator for this loss rate. This number gives an idea of the level of neutron flux. In the project, much smaller linear loss density ~5 *pA/m* suggested [1] brining neutron flux density in regular parts to very low level. So even losses of this current in 1-*m* long Aluminum target will deliver local neutron flux ~ $\dot{D}(rem/hour/m) \cong 2.16\cdot 10^{-4}$ – i.e. about three times below allowed by safety regulations.

It is interesting to compare the dose for the high-*Z* elements (Iron, Tungsten) for which the rule of thumb is

$$\dot{D}(rem/hour) \cong 2200\cdot\frac{P[kW]}{R[m]^2} \cong 2.75, \qquad (49)$$

i.e. ~6.4 times bigger. We would like to attract attention that for high-Z elements the saturated dose is not a function of *Z* in this estimation.

One other peculiarity for Graphite collimator is that the neutron source in case of soft collimation is a cylindrical one, having the length ~1 *m*. This might be

useful property for the lowering of integrated dosage to the material of collimator, if compared with Iron or Tungsten.

Now as we know the yield of neutrons expected we can move to the next step – protection from this component in radiation.

5. PROTECTION FROM NEUTRONS

According to our estimations made above, for 1*nA* losses in the collimator the dose rate calculated with (48) for Carbon at the distance *R*=2*m* for 5 *GeV* beam is $\dot{D} \cong 0.43\, rem/hour$. As the safe level lies $\dot{D}_{safe}$<0.1 *rem/week* or $\dot{D}_{safe} \le 0.1/7/24 \cong 6 \cdot 10^{-4}\, rem/hour$, the attenuation required is ~716 times, i.e. a moderate one. Also the losses of 1 *nA* could be considered as majorette one; in ERL project the looses expected at the level 200-1000 times lower. This dose calculated for permanent exposure of personnel; in reality the exposure time might be less also.

But main conclusion is that in mostly places where the losses estimated <1*pA/m* the protection shield dos not required at all, as the corresponding dose here is $\dot{D} \cong 4.3 \cdot 10^{-4}\, rem/hour < D_{safe} = 6 \cdot 10^{-4}\, rem/hour$. For losses 5*pA/m* the protection shield must deliver attenuation ~3.5 times.

Detailed description of neutron interaction with media is given in [13]. Thermal diffusion length (L_D) is the characteristic distance between the point at which a neutron becomes thermal and the point of its final capture. Thermal neutrons have about the same energy as the surrounding matter, typically < 0.4 *eV* (0.025 *eV* at 300^{o}K).

So, the basic strategy against neutrons has few distinct steps, which are the following.

First it is in reduction the energy of electrons as much as possible before it reaches the productive media; *second*-neutrons must be moderated to low, basically thermal energy; *third*- the neutrons could be absorbed by Boron/Cadmium rich media. Overall protection shield made from Lead guaranties the reduction of any leak of dangerous radiation outside the collimator region. This outer Lead shield combined from standard-size bricks could be extended, if necessary, is sensitive directions to protect personnel working area. Lead support must be designed so it allows installation of additional bricks.

For description of process of moderation, the variable $\eta = \ln\frac{E_0}{E}$, introduced earlier for description of processes in shower in (19), is broadly in use for description of diffusion and moderation of neutrons and called the *lethargy*. Here E_0 stands for the reference energy and *E* stands for current neutron energy. As we mentioned, the lethargy η allows to find energy as $E = E_0 \exp(-\eta)$.

Table 4 [13]. Some parameters used for neutron moderation calculations: τ_T –age of thermal neutrons, L_S–moderation length, L_D–diffusion length.

Media →	H_2O	C	Fe	Pb	SiO_2	B_4C
ρ, g/cm^3	1[6]	2.25	7.84	11.36	1.6	2.52
τ_T, cm^2	27.7	364	1570	7100	2300	174
L_S, cm	5.25	19.0	39.6	84.2	48.0	13.2
L_D , cm	2.85	54.5	1.32	13.5	30.3	0.02

Usual or light water absorbs neutrons, but for our purposes this is a useful property (in contrast to nuclear reactor business, where the heavy water, which does not absorb neutrons, is in use for the moderation). The same is true for any moderator used for our purposes. The enlargement of water cooling jacket could be done to some extent without any problem, as the water flow (and pressure) required for cooling is very low (water needs to carry out few watts only). Moderation length for water is ~5 *cm* so one moderation length jacket looks adequate here.

Polyethylene and paraffin (including liquid paraffin) are among the best candidates for slowing neutrons also. The neutrons flux in not high, so the lifetime of polyethylene is not an issue here. Modular design allows fast replacement in case of damage.

Carbon in collimator also moderates neutrons from the very beginning. Pure Beryllium moderator looks expensive for our business; however as Beryllium fluoride salt (FLiBe) is possible also, although it looks rather exotic for accelerator practice.

Numerous experiments indicate, that spatial distribution of neutron flux density could be described pretty accurately with the help of exponential function

$$\varphi(\tau) = \varphi_0 \cdot \exp(-\tau / L_R), \tag{50}$$

where L_R –is so called the relaxation length associated with material of protection shield [13]. This value has clear physical meaning –namely it indicates the distance, at which the flux drops *e* times. If the protection shield composed from different materials, attenuation could be described as a product of exponential factors with its specific values of relaxation length $L_{R,i}$ and thickness τ_i,

$$\varphi(\tau) = \varphi_0 \cdot \exp(-\sum_{i=1}^{m} \frac{\tau_i}{L_{R,i}}) \tag{51}$$

In Tables 5, 6 relaxation lengths represented for some materials used for neutron protection.

[6] Partial density of Hydrogen in water is $\rho_H \cong 0.111 g/cm^3$

Table 5.[13]. Relaxation length L_R for neutrons with energy E=4MeV

Media →	H_2O	C	Fe	Pb	Polyethylene	B_4C
ρ, g/cm^3	1	2.25	7.84	11.36	0.92	2.52
L_R, g/cm^2	6.2	19	59.5	169	5.05	20
$l_R = L_R / \rho$, cm	6.2	8.4	7.5	14.9	5.4	7.9

Table 6. Relaxation length L_R for energy E~14-15MeV

Media →	H_2O	C	Fe	Pb	Polyethylene	B_4C
ρ, g/cm^3	1	2.25	7.84	11.36	0.92	2.52
L_R, g/cm^2	14.2	32.9	64.2	173	12.8	28.8
$l_R = L_R / \rho$, cm	14.2	14.6	8.2	15.2	13.9	11.42

One can see that Iron is about twice more effective for attenuation of fast neutrons per unit length, than Lead in wide energy area of neutron spectra. Value L_R could be treated also as a weight of material with cross section area 1 cm^2, delivering attenuation of neutron flux e times. Again, Iron-made protection shield has advantages over Lead one about 2.7 times, if compared by the weight. One negative factor associated with Iron is in its easy magnetization, sometime in unpredictable way. If inside the iron shield magnetic field level could be kept controllably low, at the edges in fringe area this might be problematic. As we do not expect thick protection shields as the losses in ERL are low, we prefer for the moment Lead wrap for collimator, as it adds more attenuation for gammas, ~Z^2 at high energy.
Formulas (50), (51) in some sense are integrated ones which take into account real attenuation in media, what includes moderation and absorption.
We would like to underline here, that protection shield is not a part of collimator itself, although it is useful to keep in mind the overall weight/size of protection system *and* collimator.

6. COLLIMATOR DESIGN

Collimators for photons and electrons have lot of components in common. Overall size depends on energy of incident beam. For any type of collimator lowering neutron flux is one of primary goals. For electron collimator, as a rule, the quality of collimated beam is important issue, as the collimated electron (positron) beam used further in low-aperture magnetic radiators or collision systems (like in IP of ILC). As attenuation of gamma-flux is few times smaller, than attenuation of electron one, the photon collimator requires bigger longitudinal size typically.

Again, very crucial for collimator is an ability to withstand direct hit of the main beam train. As the emittance of the beam is very small ($\gamma\varepsilon_{x,y} \leq 1mm \cdot mrad$) the beam size might be ~30-50 μm accepting energy ~4 *kJ*.

6.1 Electron collimator. So the basic concept put in grounds of electron collimator design emerges as the following. *First*, materials which potentially could be hit by the beam/bunch are made from lightweight (low *Z*) media. *Second*, attenuation of neutron flux and neutron absorption made in a separated protective shield which is not a part of collimator itself. As we would like to be sure, that mostly of shower located inside media, the transverse size of collimator can reach one Molière radius, ~4.8 *cm* for Graphite.

Special attention needs to paid to avoid resonance RF frequencies around 1.3 *GHz*.

Let us consider a collimator represented in Fig.5. Pyrolithic Graphite (PG) is used as a low *Z* material, although we do not exclude usage of ordinary Graphite-Crystalline or Synthetic ones sequencing PG after some distance.

PG manufactured by decomposition of a hydro-carbon gas at very high temperature in a vacuum furnace. PG is available as plates, tubes etc. with its properties strongly dependent on direction. Graphite absorber body split in many parts as thick washers with high thermal conductivity in direction to the cooling wall. Graphite washers inserted into the tube with lapping and brazed into Copper tube or with thread. The Copper tube is cooled by a liquid, running in a surrounding jacket. Graphite disk has an axial hole of ~5mm in radius.

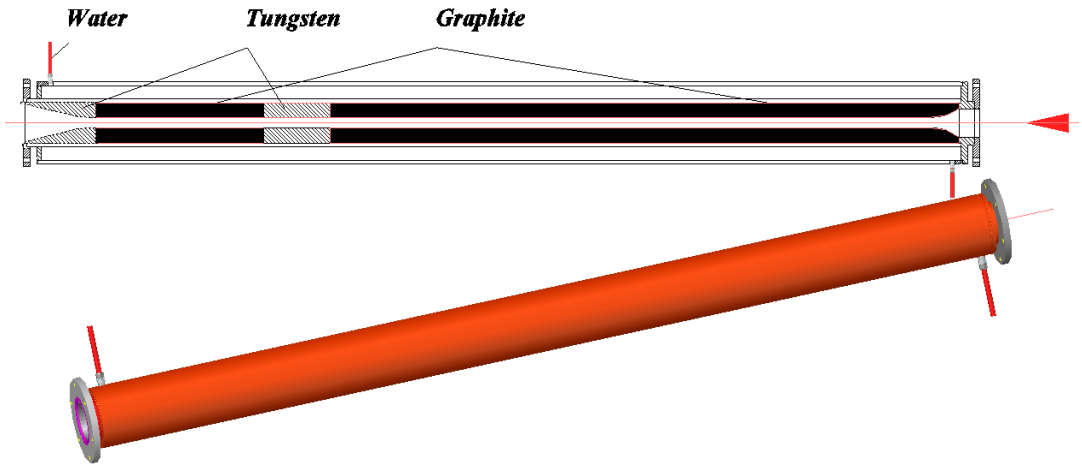

Figure 5: Collimator with Graphite. ***Beam is coming from the right.*** Flanges are 4 inch in diameter. Overall length of collimator had shown ~150*cm*. Long Graphite cylinder assembled by many discs having a hole at the center.

After Graphite front-end insertion installed a Tungsten (Tungsten alloy, more exactly) cylinder technologically made as a long nut, in the same Copper tube. Tungsten cylinder has the hole of the same diameter as the Carbon one. For

making a hole in Tungsten cylinder, having the length~5 *cm* it either is sectioned in longitudinal direction or split in halves along the beam line. Anyway technology of making small-size holes in long Tungsten materials exists[7]. Inside the copper jacket, the Tungsten enclosure is fixed by thread. It will be not a problem to make a thread inside tube having ~8*cm*.

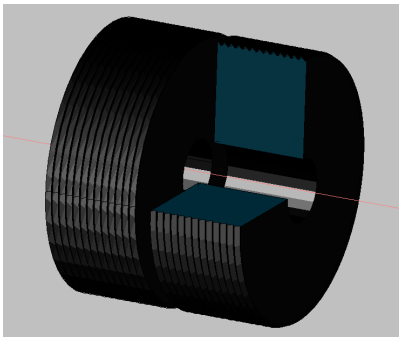

Figure 6: A fragment of PG collimator. Threaded thick washers have good conductivity plane oriented across the collimator axis.

For reduction of resistive wake-field effect, the surface of Graphite washes is galvanized by few micron thick layer of Copper, so after assembling the sides looking to the beam arrange a well conducting surface[8].

Water cooling system (water jacket) has extended thickness ~5cm, which corresponds to one moderation length (see Table 4).

PG has unique properties, such as high temperature of operation, as it is stable up to 3000^{o}C, low vacuum outgassing and the heat conductivity ~400 *W/m-*^{o}*K* (directional, in rectangular plane -3.5 *W/m-*^{o}*K*) which is comparable with Copper. For Graphite, $l_{X_0} \cong 19.2$ *cm* (X_0 =43.3 *g/cm*^{2}). The graphite cylinder, as we mentioned above, made in sections which high conducting plane oriented rectangular to the collimator axis. Carbon fiber reinforcement is possible.

We would like to attract attention that thermal conductivity of PG HT graphite is ~four times of Copper (what is ~400 *Watts/Meter/*^{o}*C*) in a plane across the surface. Sublimation of PG investigated for usage as a target for muon production [7]. For temperatures > 3650^{o}C sublimation in vacuum is going from one side of cylindrical hole to another, so formally there is no losses of material. Cross section of all set is shown in Fig. 7.

Expected neutron flux defined by the losses of electrons in media of collimator (which was estimated as 5*pA*). Basically the losses defined by electro-optical functions at collimator location, but still, for emittances under consideration in ERL the transverse beam sized defined by this factor is too small; for

[7] Used for making collimator for E-166 with inner diameter hole 0.7mm and length~100mm.

[8] For collimation of gammas in positron conversion system of ILC the electrical conductance of Graphite is not important at al.

$\gamma\varepsilon \cong 10^{-5}\, cm \cdot rad$, $\beta \cong 10m = 1000cm$, $\sigma_{\perp} \cong \sqrt{\gamma\varepsilon \cdot \beta / \gamma} \cong 10^{-3} cm = 10\mu m$, so diameter of collimator d=10 *mm* corresponds to 10*mm*/20 μm ~5000 sigma.

Table 7. Properties of PG

Graphite →	PG SN	PG HT
Density	2.18 - 2.22 g/cm^3	2.22 g/cm^3
Flexural Strength (A* plane)	18 *kpsi* (120 *M Pa*)	4.8 *kpsi*
Tensile Strength (A plane)	12 *kpsi* (80 *M Pa*)	4.2 *kpsi* (29 *MPa*)
Compressive Strength (A plane)	15 *kpsi* (105 *M Pa*)	
Young's Modulus (A plane)	3 x 10^6 *psi* (20 *GPa*)	7.2 *Mpsi* (50 *GPa*)
Thermal Exp. Coeff. (A plane)	0.5 x 10^{-6} *cm/cm/*°C	-0.6·10^{-6} *cm/cm/*°C
Thermal Exp. Coeff. (C* plane)	6.5 x 10^{-6} *cm/cm/*°C	25·10^{-4} *cm/cm/*°C
Thermal Conductivity (A plane)	400 W/m/ °C	1400 *W/m/* °C
Thermal Conductivity(C plane)	3.5 W/m/ °C	7 *W/m/* °C
Electrical Resistivity (A plane)	5 10^{-4} *ohm·cm*	5 10^{-4} *ohm·cm*
Electrical Resistivity(C plane)	0.5 *ohm·cm*	0.6 *ohm·cm*
Crystal Structure	Hexagonal	
C/2 Spacing):	3.42 Å)	
Outgassing	non	non

*A –along basal planes; C-through basal planes (thickness)

Dispersion function at collimator location is zero for the starting point coinciding with the entrance of return loop, so the only energy spread input to the beam size arises from IBS in return loop region. For estimation of this energy spread increase rate, first we would like to underline, that the rate of scattering for 90° in CM system for multiple and single act process ratio is

$$\frac{\text{Rate for multiple scattering for } 90^{\circ}}{\text{Rate for single act scattering for } 90^{\circ}} \cong 8Ln_C \,, \tag{52}$$

where

$$Ln_C = ln\frac{a_{max}}{a_{min}} \cong ln\sqrt{\frac{(v'/c)^6}{4\pi r_0^3 n'}} \tag{53}$$

is Coulomb's integral, n' is the bunch density in a moving frame, v' stands for the speed of transverse motion in a moving frame.

Formula for the speed of diffusion by small-angle scattering in a moving frame, where velocity of transverse motion is dominant can be expressed by simple formula

$$\frac{dp'^2}{dt'} = \frac{4\pi e^4 n' Ln_C}{v'} \,, \tag{54}$$

which could be transformed in Lab system for the betatron size dominance $\varepsilon_x \beta_x \geq (\eta \Delta p_{\|} / p)^2$, as the following

$$\frac{d(\Delta E / E)^2}{ds} \cong \sqrt{\frac{2}{\pi}} \frac{L n_C N r_0^2}{\gamma^3 \cdot \varepsilon_x \cdot \sigma_s \cdot \sqrt{\varepsilon_x \beta_x}} \tag{55}$$

Substitute here for estimations $\beta_x \cong \beta_y \cong 10\text{m}$; emittance (not invariant) $\varepsilon_x \cong \varepsilon_y \cong 3 \cdot 10^{-9}\text{cm}\cdot\text{rad}$, $N \cong 10^9$ (i.e. 160*pQ per bunch*), $\sigma_s \cong 0.06cm$ (2*ps*), $\gamma \cong 10^3$ (500*MeV*), one can obtain $\frac{d(\Delta E / E)^2}{cdt} \cong 2 \cdot 10^{-14}[1/cm]$. After passage of full return loop having circumference~20000*cm* this could raise the energy spread up to $\sqrt{(\Delta E / E)^2} \cong 2 \cdot 10^{-5}$.

Let we majorette the beam size generated by the energy jump generated in the return arc and transferred to the entrance of collimator (where it must be zero, if counted from the entrance of the arc) as

$$\Delta x \cong \eta_{\max} \cdot (\Delta E / E).$$

Estimate $\eta_{\max} \cong R \cdot (1 - Cos\frac{\pi}{n_{per}})$, where R stands for the bending radius of magnets in arc, n_{per} –is the number of periods in arc. For $n_{per} = 10$, $R \cong 10m$, one can obtain $\eta_{\max} \cong 1000 \cdot (1 - Cos\frac{\pi}{10}) \cong 49cm$ and $\Delta x \cong 10^{-3} cm$, i.e. again the size, comparable with the betatron one. So the losses of the beam current at collimator location are extremely low under quiet conditions and the mostly function of collimator remains –its protection SRF module from SR of bending magnet.

Now let us come back to the description of collimator which cross section represented in Fig.7.

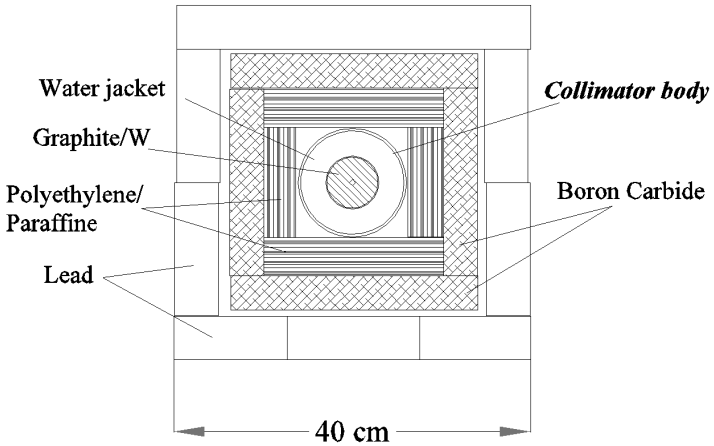

Figure 7: Cross section of collimator *with* surrounding neutron protection shield. Inner diameter of aperture is ~10mm. Lead shield could be extended, if necessary, in any direction towards the personnel working area.

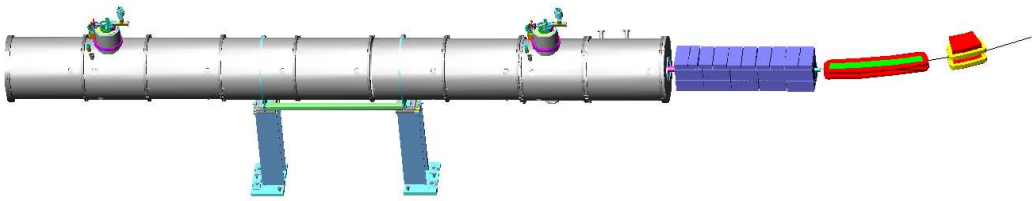

Figure 8: SRF module, collimator covered by shield, sectioned bending magnet at the end of returning arc.

Water jacket serves two purposes: cooling and slowing down neutrons, although the thickness of water jacket is not enough for full-scale moderation. Some low *Z* material (Polyethylene) could wrap the body of collimator in addition to the shown.

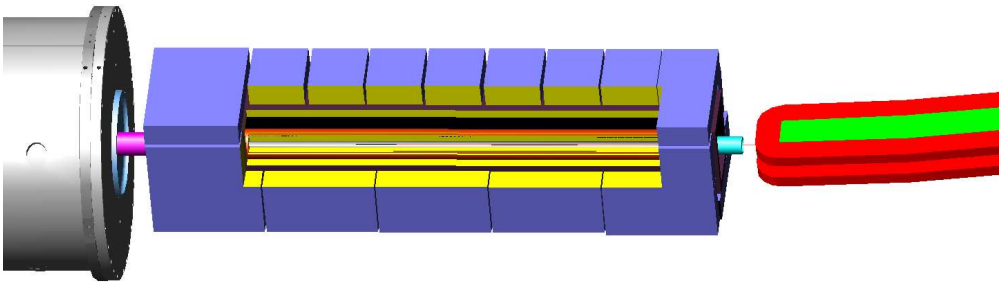

Figure 9: Scaled view on the fragment of Fig.8.

Boron Carbide (B_4C) is produced in tonnage quantities, so there is no problem in acquiring necessary amount.

In addition to passive absorption and scattering one can suggest an installation behind this collimator another one, made as the Iron cylinder with central hole bigger, than the one in a Carbon/W collimator. This additional collimator with Iron magnetized in azimuthtal direction supposes to bend charged tailored secondary particles inside the iron out from forward direction. In this geometry the azimuthtal induction B~15-20 *kG* can be reached with a small axial current running in cylindrical Copper-made enclosure coaxial with central vacuum chamber (or even through the Iron). Again, the main problem with such type of collimator associated with fringe fields.

6.2. Photon Collimator. As we mentioned, attenuation of gamma-flux (see Fig.10) is less, than attenuation of electron beam (~2MeV/g/cm-^{2}), as the photons, must be transform theirs energy to electrons by Compton scattering. Then these electrons loose its energy either by ionization of media or by pair creation.

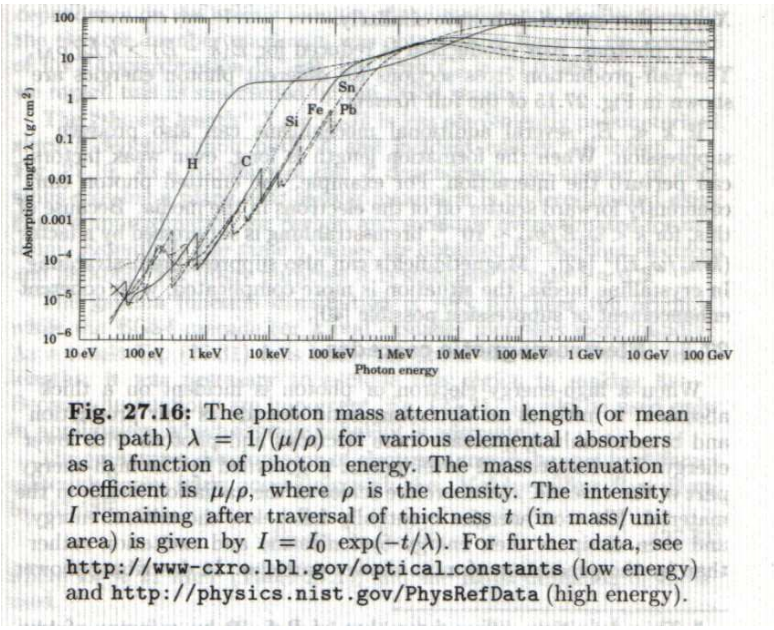

Fig. 27.16: The photon mass attenuation length (or mean free path) $\lambda = 1/(\mu/\rho)$ for various elemental absorbers as a function of photon energy. The mass attenuation coefficient is μ/ρ, where ρ is the density. The intensity I remaining after traversal of thickness t (in mass/unit area) is given by $I = I_0 \exp(-t/\lambda)$. For further data, see `http://www-cxro.lbl.gov/optical_constants` (low energy) and `http://physics.nist.gov/PhysRefData` (high energy).

Figure 10: Attenuation of gammas in different media [10].

Gamma flux in ILC positron conversion system has power up to 100*kW* DC and energy spectrum is limited by ~100MeV. Cut off frequency of the first undulator harmonics lies in ~15 *MeV*, but the main purpose of collimator here-to cut second and higher harmonics as they reduced polarization of the photon flux. From Figure 10, the photon mass attenuation length for ~20 MeV photons is ~60 g/cm^2. So for carbon this will correspond to ~120 cm length which will reduce the photon flux ~3 times only. So for increase efficiency of system one can introduce thin baffles of high Z material (having low critical energy), which will help to convert the photons into electron-positron pairs, which now be moderated in low Z media. In positron production system of ILC, the baseline for target is a Ti, which has ~0.5X_0 , so the gamma-beam loses ~15% of its flux. As collimator must cut (absorb) ~50% of all 100*kW* (max), distribution of these losses in volume is necessary for reduction of thermal stress. So we came to combination of PG and Ti baffles, Fig 11. The thickness of baffles may vary from thin at the entrance to the thick at the exit. The photons affected (scattered) by collimator does not affect efficiency of conversion system.

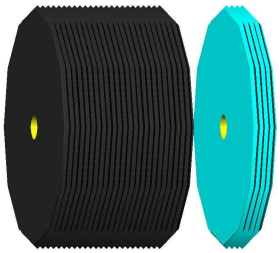

Figure 11: PG and Ti discs.

Again, PG discs have good electric and thermal conductivity across in direction to the threaded side. All components of collimator are shown in Fig. 12.

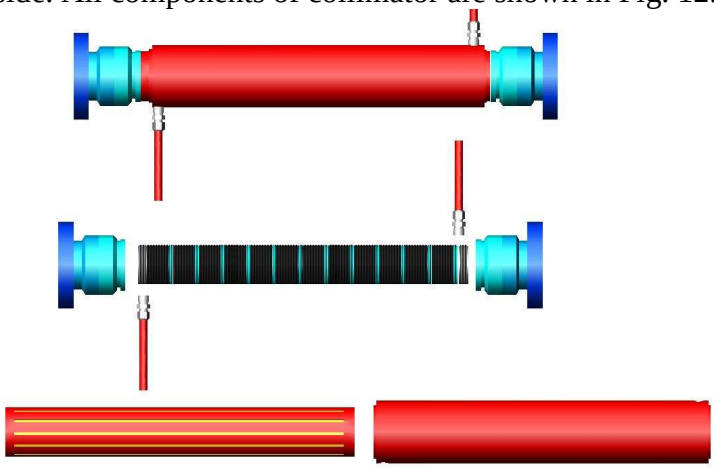

Figure 12: Structure of high-energy gamma-collimator for high power beam.

The same principle can be used in design of baffled collimator for wigglers or undulators which are planned at ERL.

7. BEAM DUMP

Again, the beam dumps for electron and photon beam, like collimators, have a lot of in common. However, to be absorbed, the gamma beam first needs to be transformed into electrons/positrons. This needs to be done gently, without exceeding allowable power density. One other difference is that for electron/positron dump, the sweeping procedure might be extremely effective, while for gammas the sweep across the target could be obtained only by mechanical sweep of absorber itself. Meanwhile sweeping helps only in distributing the average power over the large area (volume), but it is useless against heating, caused by incidence of a single train, even bunch.

Below we are considering the electron dump for ERL as example and then a gamma dump for ILC positron conversion system.

7.1. Electron Dump. Beam dump in ERL designed so it is able to accept 15 MeV beam with 0.1A DC current, i.e. ~1.5 MW of CW power or E_{tot} =1.5 MJ per second. Water flow ~5 Liters per second could be considered as absolute minimal amount required here for temperature jump ~70^{o}C as $\dot{m} \cong \frac{E_{tot}}{\Delta T C_p} \cong \frac{1.5 \cdot 10^6}{70 \cdot 4.18 \cdot 10^3} \cong$ 5.12kg/sec. Two stage cooling system more likely required here similar to what it is done in nuclear reactors.

In inner cooling loop such coolant as PbBi alloy (melt temp ~154^{o}C) could be used. Some fraction of energy could be deposited directly into PbBi coolant.

Water used in outer loop. For pumping PbBi coolant there are well developed techniques with magneto dynamical pumps. Ordinary StSteel gear pump could be used here as well.

As alternative to PbBi coolant the two loop water system with vaporization cooling in first (hot) loop could be considered here as less exotic device. In case of vaporization cooling, which uses latent heat of vaporization, this amount would be the same for the external heat exchanger; the temperature 100 deg C is a minimal one in this case. BiPb coolant allows more compact design, but definitely water cooling system looks more attractive for such relatively low energy deposition, like it is in ERL case.

Again, Pyrolithic Graphite is suggested as a front end absorber. The rate of energy loss by electrons ~2 $MeV/g/cm^{-2}$ yields full energy absorption at ~5 cm distance for 15-MeV electron beam as the ionization losses are dominant here – this gives an idea of longitudinal size of Carbon required.

Single loop cooling system will require rather developed area and more likely higher thermal gradients. From the other hand such a system looks simpler.

As the energy of the beam lies below the threshold of photo-production in Graphite, neutrons expected only from inclusions of undesirable isotopes of Carbon and from irradiation of heavy elements of the case (StSteel). Two independent dump systems required more likely, while operational is the only one at every moment, keeping another one as a spare. This will reduce down period in case of repairing work at this system. Switching between them could be either mechanical or by changing the beam optics. Right now we think that simple mechanical shift of all system is a more simple way to proceed.

One important nuance here is that the bunches, arriving to the dump system, carry significant RF power, about the same as DC power of the beam. So if the dump cavity has resonant frequency nearby the 1.3 GHz, then the beam could power the dump cavity. Voltage developed could reach (or even overwhelm the energy of incident beam) producing sparking and RF burning inside the volume of dump system. So we paid attention to this possibility in our design (Fig. 13) making parasitic cavities as small as possible.

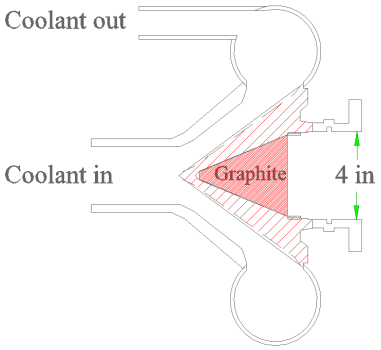

Figure 13: The concept of an electron dump system with vapor cooling in first stage. Two-phase flow comes out through peripheral tube(s). Coolant enters at the center. Entrance orifice has diameter 4 in.

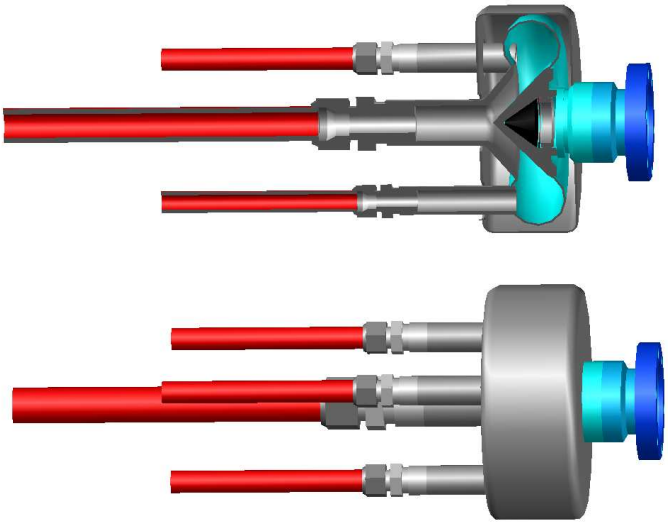

Figure 14: Isometric view on e^- beam dump.

Conical shape of graphite absorber tightened by springing nut, allows easy expansion while temperature rises as the cone shape remains alike.
The beam dump unit designed is pretty compact, having dimensions of an 1/8 of a cubic meter total (two loops system with pump).

Adequate vacuum pumping required in this region, however the PG outgassing is minimal. Safety vacuum valves required for cut the beam dump from the other system in case of emergency and for commissioning.
Blocking elements serve for protection against failure of any power supply of critical elements such as solenoid, bending magnet and sweeping device. Appropriate shielding will be required for this device.

7.2. Photon dump. This type of beam dump could be recommended for absorption of used gamma-beam in ILC conversion system. Similar system could be used for dump the radiation from insertion device(s) of ERL.

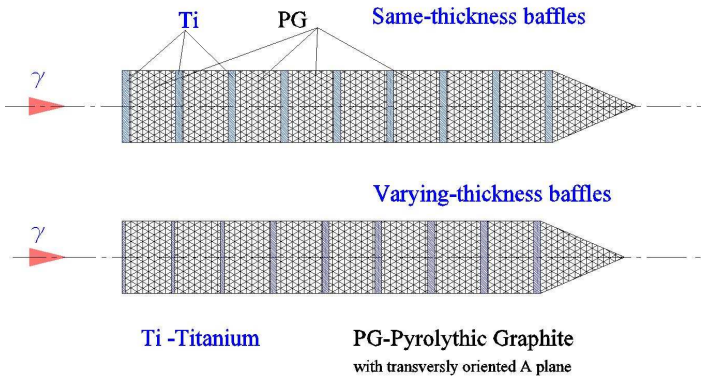

Figure 15: The concept of gamma beam dump.

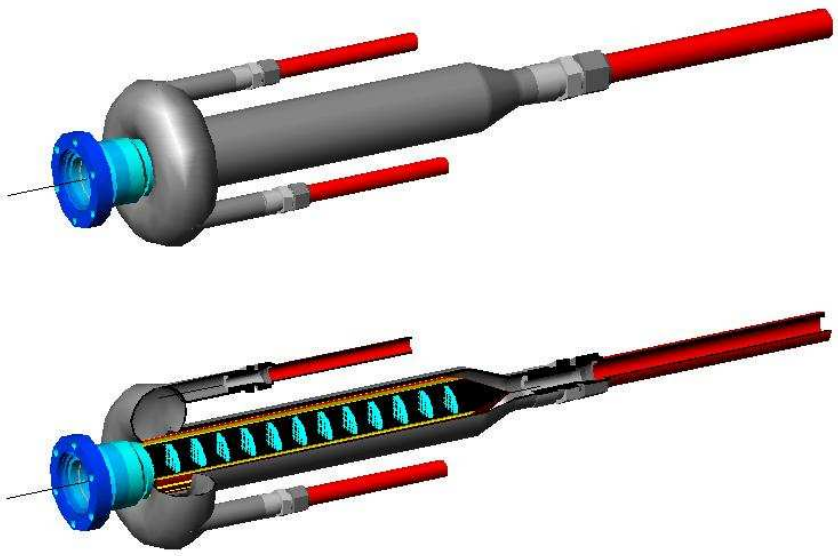

Figure 16: Isometric view on gamma-absorber.

In Figure 17 below there are shown trajectories of individual 25-*MeV* incident photons and gammas calculated with code CONVER [20].

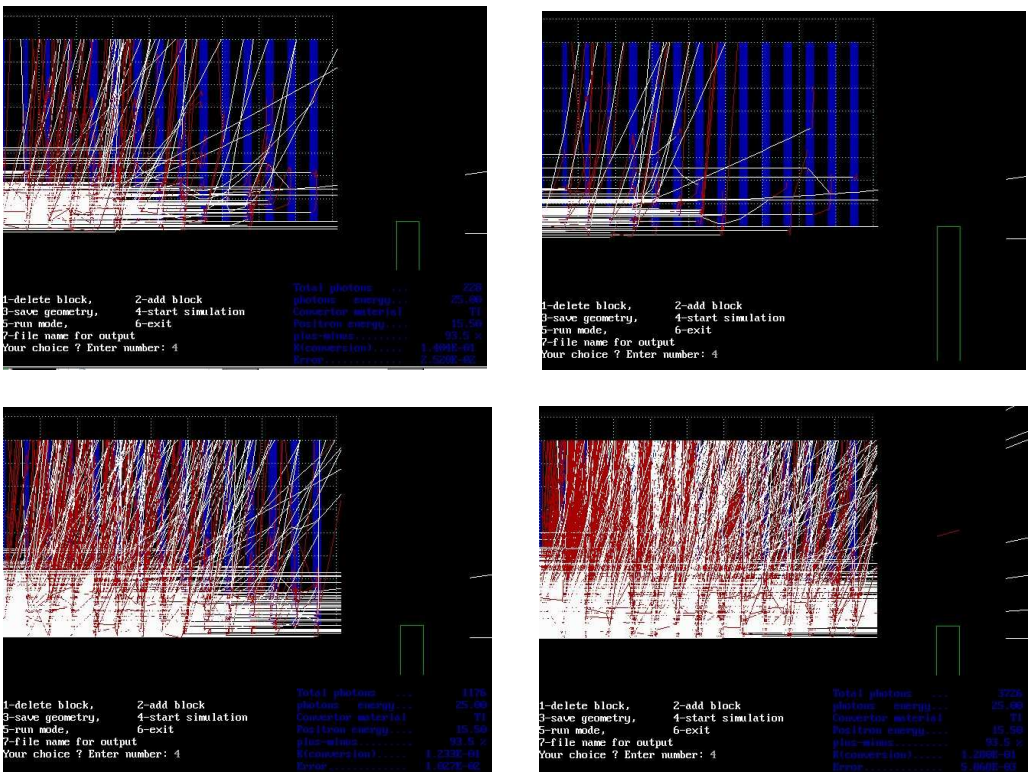

Figure 17: Trajectories of positrons (red) and gammas (white) in baffled absorber as they developed it time (from left to right, from top to bottom).

Despite the formula (48) derived for incident electrons, we can apply it to the photons, as finally all photons will be converted into electrons/positrons, so this formula we serve as majorette for the activity. Substitute Z=22, P=100kW, one can estimate for distance R=1 m

$$\dot{D}(rem/hour) \cong 93 \cdot Z^{0.73} \frac{P[kW]}{R[m]^2} \cong 93 \cdot 22^{0.73} \frac{100}{1} \cong 88.8 krem/hour\ .$$

Of cause, this is a big number, but during operation no personnel will be present around; what is important—an activation of surrounding materials induced by this neutron flux. Utilization of low Z materials is crucial here.

7.3. Electron and Gamma-beam positioning monitor

Anisotropic electric conductivity of PG allows elegant solution for gamma position monitor, Fig. 18. Standard PG disc has a cross, milled to some depth~2mm. As the electric conductivity of PG in radial direction is 1000 times bigger, than along axis, such grooves arrange segmented monitor.

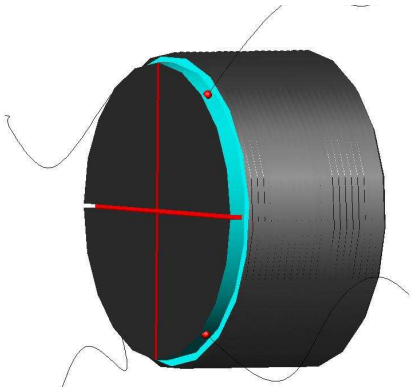

Figure 18: The gamma-beam position monitor concept. PG has low conductivity along axis. Segments arranged by narrow groves in PG body.

At the threaded surface some radial lowerings are made as it is shown in Fig.18. These lowerings metalized and each having galvanic contact with a wire, running out of absorber in a grooves. When the gamma/electron/positron beam hits the PG, electrons are knocked from segment media in longitudinal direction need to be restored, so the current is running to segment serves as the measure of amount of knocked electrons. Analyzing the difference in signals from all wires, one can restore the center of gravity of the beam centroid. *The similar device could be implemented in collimator as well.*

8. SUMMARY

Concepts put in grounds of collimator and absorber design are clear and straightforward. The basis is in making the first stage of collimator/absorber from

low *Z* material-Pyrolithic Graphite, and the second stage(s) from high *Z* material (Tungsten, Ti).

Usage of Pyrolithic Graphite allows the collimator to withstand direct hit of the beam train and make soft cut of halo. We do not exclude usage of less expensive commercial-grade graphite in combined with PG. Usage of Carbon Fiber reinforced Graphite is also possible here, as it might help withstand the shock waves induced in the collimator body.

Neutron yield reduced by usage of Graphite as a beam stopper at first, and then by the usage of water and Hydrogen saturated paraffin/polyethylene for moderation of neutrons, and, finally, by usage of Boron Carbide for low energy neutron absorption. Lead housing wraps the collimator system. Usage of Iron as a material for protecting shield requires careful consideration of fringe fields associated with this easily magnetized media.

The collimator installed *in front of South linac* serves for halo cut and for protection of SRF module from exposure to SR. Similar collimators installed at the *entrance of North linac* combined with fast kicker serves for protection of North SRF module triggered by failure of electron source and in case of emergency. *Design of such fast kicker will be described in a separate publication*. So these two collimators look as minimal required pair for ERL.

One additional collimator could be installed also in front of ERL Demerger. Small aperture of collimator $\leq 10mm$ in diameter allow prevention of SRF module, as SR touches module at significant distance from the entrance of SRF module, so the requirements for the bending field strength could be reduced.

Insertion devices could be protected by this type of collimator also[9].

A concept for the beam dump considered here; this dump is able to absorb 1.5 *MW* of DC power. It is also could be used in gamma-beam dump of ILC, for absorption of up to 100kW of gamma flux, generated mostly by first harmonic with energy of photon ~18 *MeV*. So as this energy is below the threshold of (γ, n) reaction for Carbon the neutron flux expected will be low also.

So the general conclusion for ERL is that in case of stationary ("quiet") conditions, where the losses majoretted by 5 *pC/m*, the dose generated by such losses is well within allowed, so collimators required in the system only for some critical situation, inevitable in long term exploitation.

One additional possibility for reduction of exposure of personnel in ERL complex might be in installation of beam channels elevated, above the human height and utilization of thin lead protection sheets, wrapping the vacuum chamber.

[9] Latest design of undulator with SC conductor allows having helical undulator with period ~25*mm*, open aperture ~10*mm* and *K*~1.0 with the possibility to change polarization by changing current in set of helical windings.

9. REFERENCES

[1] G.H. Hoffstaetter, I.V. Bazarov, S.A. Belomestnykh, D.H. Bilderback, M.G. Billing, G.W. Codner, J.A. Crittenden, B.M. Dunham, M.P. Ehrlichman, K.D. Finkelstein, M.J. Forster, S. Greenwald, S.M. Gruner, V.O. Kostroun, Y. Li, M.U. Liepe, C.E. Mayes, H.S. Padamsee, S.B. Peck, D.H. Rice, D.C. Sagan, Ch. Spethmann, A.B. Temnykh, M. Tigner, Y. Xie, "*Challenges for Beams in an ERL extension to CESR*", MOPC056, Proceedings of EPAC08, Genoa, Italy, pp.190-192,2008 , Report Cornell ERL08-3, 2008.

[2] G.H.Hoffstaetter, T.Tanabe," *Reducing Radiation on RF Cavity Surfaces in the Proposed Cornell Energy-Recovery Linac*", Report Cornell ERL04-2, 2004.

G.H.Hoffstaetter, M.Liepe, T.Tanabe, *"Reducing Radiation on RF Cavity Surfaces in an Energy-Recovery Linac*", EPAC2004, Lucerne, CH; ERL04-6.

[3] A.A.Mikhailichenko, "*Longitudinal Damping System with two Transverse Kickers*", CBN 96-10, Cornell 1996.

Also: PAC03, Portland, Oregon, 12-16 May 2003, Proceedings, p.2781.

[4] A.A.Mikhailichenko, "*Collimator for ILC*", EPAC2006, Edinburgh, UK, June 26-29 2006, MOPLS105, Proceedings, pp.807-809.

[5] S. Hayakawa, "*Cosmic Ray Physics*", Wiley-Interscience, 1969.

[6] T.A.Vsevolojskaya, A.A.Mikhailichenko, G.I.Silvestrov, A.N.Cherniakin, "*To the Project of Conversion System for Obtaining Polarized Beams at VLEPP Complex*", internal report BINP, Novosibirsk, 1986.

[7] J.R.Haines, C.C. Tsai, P.T. Spampinato, "*Summary of Graphite Sublimation Tests*", Neutrino Factory and Muon Collider Collaboration Meeting, Shelter Island, NY, May 9-15, 2002.

[8] M.I. Aizatskiy, A.M. Dovbnya, I.M. Prokhorets, S.I. Prokhorets, Y.V. Rudychev, M.A. Khazhmuradov, "*Mathematical Modeling of a Neutron Production Target of an Electron Accelerator Driven Subcritical Assembly*", Problems of Atomic Science and Technology. 2006. № 2, *Series:* Nuclear Physics Investigations (46), p.28-30.

[9] V.I.Noga, Yu.N.Banyuk, Yu.N.Telegin, "*Photoproduction of neutrons in a Thick Target*", Translated from Atomnaya Energiya, Vol. 47, No. 3, pp. 183–184, September, 1979.

[10] *Particle Physics Booklet*, Particle Data Group, LBNL, Berkeley, CA 94720-8166.

[11] W.P.Swanson, "*Calculation of Neutron Yields Released by Electrons Incident on Selected Materials"*, Health Physics, Vol.35, pp.353-367, 1978.

[12] I. Tamm, S.Belen'ky, "*On the Soft Component of Cosmic Rays at Sea Level*", J.Phys.(U.S.S.R.) **1**, 177 (1939).

[13] N.G.Gusev, V.P. Mashkovich, A.P.Suvorov, *"Physical Foundations for Protection against Radiation*", Moscow, Atomizdat, 1980, Vol. 1, 461 pp., (in Russian).

[14] G.Bathlow, E.Freytag, K.Tesch, "*Measurements on 6.3 GeV Electromagnetic Cascade-Produced Neutrons*", Nucl. Phys. **B2**, 669(1967).

[15] B.L.Berman, "*Atlas of Photoneutron Cross Sections Obtained with Monoenergetic Photons*", Bicentennial Edition, LLL, Report No.UCRL-78482 (1979), also in Atom. Data &Nucl Data Tables **15**, 421(1975).
[16] L.W.Jones, K.M.Terwilliger, "*Photoneutron Production Excitation Functions to 320 MeV*" Phys. Rev. **91**, 699(1953).
[17] R.Montalbetti, L.Katz, J. Goldemberg, "*Photoneutron Cross Sections*", Phys.Rev. **91**, 659 (1953).
[18] Ya.B.Zeldovich, Yu.P.Raizer," *Physics of Shock Waves and High-Temperature Hydrodynamic Phenomena*", Vol.II, Academic Press Inc. 1967.
[19] See http://physics.nist.gov/PhysRefData .
[20] A.D. Bukin, "*Choice of Optimal Positron Converter for Low Energy Beam*" (in Russian), Preprint INP 90 –100,Novsibirsk, 1990.